Article

Pressure Response of Three-Dimensional Cyanide-Bridged Bimetallic Magnets

Masaaki Ohba, Wakako Kaneko, Susumu Kitagawa, Takuho Maeda, and Masaki Mito

J. Am. Chem. Soc., **2008**, 130 (13), 4475-4484 • DOI: 10.1021/ja7110509

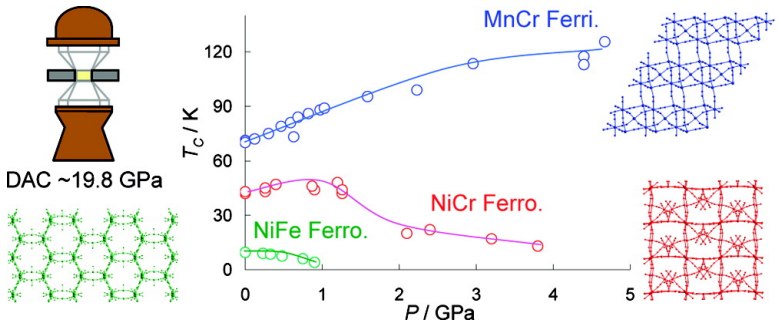

More About This Article

Additional resources and features associated with this article are available within the HTML version:

- Supporting Information
- Links to the 1 articles that cite this article, as of the time of this article download
- Access to high resolution figures
- Links to articles and content related to this article
- Copyright permission to reproduce figures and/or text from this article

View the Full Text HTML

J|A|C|S
ARTICLES
Published on Web 03/11/2008

Pressure Response of Three-Dimensional Cyanide-Bridged Bimetallic Magnets

Masaaki Ohba,*,† Wakako Kaneko,† Susumu Kitagawa,†,‡ Takuho Maeda,§ and Masaki Mito*,§

Department of Synthetic Chemistry and Biological Chemistry, Graduate School of Engineering, Kyoto University, Katsura, Nishikyo-ku, Kyoto 615-8510, Japan, Institute for Integrated Cell-Material Sciences (iCeMS), Kyoto University, 69 Konoe-cho, Yoshida, Sakyo-ku, Kyoto 606-8501, Japan, and Faculty of Engineering, Kyushu Institute of Technology, Kitakyushu 804-8550, Japan

Received December 12, 2007; E-mail: ohba@sbchem.kyoto-u.ac.jp; mitoh@elcs.kyutech.ac.jp

Abstract: Effects of pressure on the structures and magnetic properties of three types of 3-D cyanide-bridged bimetallic coordination polymer magnets, $Mn^{II}Cr^{III}$ ferrimagnet $[Mn(en)]_3[Cr(CN)_6]_2 \cdot 4H_2O$ (**1**; en = ethylenediamine), $Ni^{II}Cr^{III}$ ferromagnet $[Ni(dipn)]_3[Cr(CN)_6]_2 \cdot 3H_2O$ (**2**; dipn = *N,N*-di(3-aminopropyl)amine), and $Ni^{II}Fe^{III}$ ferromagnet $[Ni(dipn)]_2[Ni(dipn)(H_2O)][Fe(CN)_6]_2 \cdot 11H_2O$ (**3**), were systematically examined under hydrostatic pressure up to 19.8 GPa using a piston-cylinder-type pressure cell and a diamond anvil cell. The ferrimagnet **1** showed the reversible crystalline-to-amorphous-like phase change, and the magnetic phase transition temperature (T_C) was reversibly changed from 69 K at 0 GPa to 126 K at 4.7 GPa. At higher pressure, the net magnetization was suppressed with increasing pressure, and the magnetic state at 19.8 GPa was assumed to be paramagnetic. The initial ferrimagnetic phase of **1** was not recovered after releasing the pressure from 19.8 GPa. The magnetic phase of **2** was reversibly converted between ferromagnetic and paramagnetic-like phase in the range $0 \leq P \leq 4.7$ GPa while maintaining its crystallinity. The porous ferromagnet **3** was easily amorphized and irreversibly lost the ferromagnetic phase under low pressure ($P \leq 1.0$ GPa). The flexible cyanide-bridged magnetic frameworks demonstrate well the pressure response as a reflection of differences in the magnetic structure and the framework strength in the GPa range.

Introduction

Creation of multifunctional material is a current attractive challenge in the field of solid-state physics and chemistry.[1−10] To attain multifunctionality using a uniform compound, it is necessary to consider how to design such compounds and how to incorporate specific properties, such as magnetism, optical activity, ferroelectricity, electric conductivity, and so on. Coordination polymers (CPs) have attracted much attention this decade because of their characteristic structures (diversity, regularity, designability, and flexibility) and gas adsorption properties.[1,11−16] In particular, the structural flexibility allows for responses to various external stimuli (e.g., pressure, temperature, light, and guest molecules). We believe that the CPs act as a multifunction platform with leveraging of the structural flexibility. To perform multifunctionality based on CPs, incorporation of physical properties into such a flexible framework is a promising strategy. In this respect, we have systematically prepared coordination polymer magnets (CPMs), so-called molecule-based magnets, to provide multifunctionality with magnetic output responsive to external stimuli.[17−21] CPMs are

† Department of Synthetic Chemistry and Biological Chemistry, Kyoto University.
‡ Institute for Integrated Cell-Material Sciences, Kyoto University.
§ Kyushu Institute of Technology.

(1) Kitagawa, S.; Kitaura, R.; Noro, S. *Angew. Chem., Int. Ed.* **2004**, *43*, 2334.
(2) Maspoch, D.; Molina, S. R.; Veciana, J. *Chem. Soc. Rev.* **2007**, *36*, 770.
(3) Wang. Z.; Zhang. Y.; Liu, T.; Kurmoo, M.; Gao, S. *Adv. Funct. Mater.* **2007**, *17*, 1523.
(4) Cui, H.; Wang, Z.; Takahashi, K.; Okano, Y.; Kobayashi, H.; Kobayashi, A. *J. Am. Chem. Soc.* **2006**, *128*, 15074.
(5) Yamashita, M.; Takaishi, S.; Kobayashi, A.; Kitagawa, H.; Matsuzaki, H.; Okamoto, H. *Coord. Chem. Rev.* **2006**, *250*, 2335.
(6) Nuida, T.; Matsuda, T.; Tokoro, H.; Sakurai, S.; Hashimoto, K.; Ohkoshi, S. *J. Am. Chem. Soc.* **2005**, *127*, 11604.
(7) Niel, V.; Thompson, A. L.; Muñoz, M. C.; Galet, A.; Goeta, A. E.; Real, J. A. *Angew. Chem., Int. Ed.* **2003**, *42*, 3760−3766.
(8) Halder, G. J.; Kepert, C. J.; Moubaraki, B.; Murray, K. S.; Cashion, J. D. *Science* **2002**, *298*, 1762.
(9) Coronado, E.; Galán-Mascarós, J. R.; Gómez-García, C. J.; Laukhin, V. *Nature* **2000**, *408*, 447.
(10) Sato, O.; Iyoda, T.; Fujishima, A.; Hashimoto, K. *Science* **1996**, *272*, 704.
(11) Maji, T. K.; Matsuda, R.; Kitagawa, S. *Nat. Mater.* **2007**, *6*, 142.
(12) Bradshaw, D.; Warren, J. E.; Rosseinsky, M. J. *Science* **2007**, *315*, 977.
(13) Matsuda, R.; Kitaura, R.; Kitagawa, S.; Kubota, Y.; Belosludov, R. V.; Kobayashi, T. C.; Sakamoto, H.; Chiba, T.; Takata, M.; Kawazoe, Y.; Mita, Y. *Nature* **2005**, *436*, 238.
(14) Férey, G.; Mellot-Dranznieks, C.; Serre, C.; Millange, F.; Dutour, J.; Surblé, S.; Margiolaki, I. *Science* **2005**, *309*, 2040.
(15) Zhang, J.-P.; Lin, P.-P.; Zhang, W.-X.; Chen, X.-M. *J. Am. Chem. Soc.* **2005**, *127*, 14162.
(16) Yaghi, O. M.; O'Keeffe, M.; Ockwig, N. W.; Chae, H. K.; Eddaoudi, M.; Kim, J. *Nature* **2003**, *423*, 705.
(17) Kaneko, W.; Kitagawa, S.; Ohba, M. *J. Am. Chem. Soc.* **2007**, *129*, 248.
(18) Shiga, T.; Ōkawa, H.; Kitagawa, S.; Ohba, M. *J. Am. Chem. Soc.* **2006**, *128*, 16426.
(19) Inoue, K.; Kikuchi, K.; Ohba, M.; Ōkawa, H. *Angew. Chem., Int. Ed.* **2003**, *42*, 4810.
(20) Ohba, M.; Ōkawa, H. *Coord. Chem. Rev.* **2000**, *198*, 313.
(21) Ohba, M.; Maruono, N.; Ōkawa, H.; Enoki, T.; Latour, J. M. *J. Am. Chem. Soc.* **1994**, *116*, 11566.

expected to respond sensitively to structural changes with magnetic output because the magnetic interactions are measurably affected by their local bridging structure and net framework. In practice, several CPMs have accomplished reversible magnetic conversions by a solvation/desolvation process accompanied by structural transformation, where the flexible and porous framework[22−29] or removable solvent ligands[30−34] of CPMs played a crucial role. From the perspective of the structural conversion, external pressure (mechanical stress) would be more effective on CPMs than the guest molecules (chemical stimulus) and could give continuous and systematical changes.

Mechanical stress is a key stimulus to the generation of piezoelectricity and has been frequently used in research on organic conductors and magnets.[35−39] The stress is useful for controlling the electric band structures of soft organic conductors. However, ferromagnetic magnetization often disappears upon stressing organic magnets because shrinkage of the intermolecular structure mostly collapses orthogonal overlapping between magnetic orbitals of radicals and tends to favor an antiferromagnetic correlation. In the case of organic radicals that have a homo-spin system ($S = 1/2$), the pressure effect is usually not a favorable stimulus. On the other hand, with hetero-spin systems, for example, a coordination polymer ferrimagnet that is based on antiferromagnetic interaction between different paramagnetic metal ions, the stress is expected to contribute positively to magnetic characteristics. Pressure-induced internal electron transfer, spin-state transition, magnetic pole inversion, and linkage isomerism of Prussian blue analogues (PBAs) have been reported so far.[40−45] However, there have been a few attempts to apply external pressure to CPMs except for PBAs and, of course, no systematic study of the correlation among structure, electric structure, and pressure response in the GPa region.[46−53]

We have extensively studied cyanide-bridged CPMs by the use of $[M(CN)_6]^{n-}$ and coligands and have successfully prepared many CPMs with various frameworks.[17−21] Some of the cyanide-bridged CPMs showed a reversible magnetic conversion by a solvation/desolvation process, which demonstrates that the M−CN−M′ linkages and the coordination space in the frameworks are flexible and advantageous for producing environmentally responsive materials.[24−26,29−33] Here, we focus on three cyanide-bridged CPMs having a 3-D framework: $Mn^{II}Cr^{III}$ ferrimagnet $[Mn(en)]_3[Cr(CN)_6]_2\cdot 4H_2O$ (**1**; en = ethylenediamine, $T_C = 69$ K),[54] $Ni^{II}Cr^{III}$ ferromagnet $[Ni(dipn)]_3[Cr(CN)_6]_2\cdot 3H_2O$ (**2**; dipn = *N*,*N*-di(3-aminopropyl)amine, $T_C = 42$ K),[55] and $Ni^{II}Fe^{III}$ ferromagnet $[Ni(dipn)]_2[Ni(dipn)(H_2O)][Fe(CN)_6]_2\cdot 11H_2O$ (**3**; $T_C = 8.5$ K).[24,56] Each compound has a different 3-D framework and magnetic properties. In particular, compounds **1** and **2** exhibit high T_C among structurally characterized CPMs. Here, we report reversible and irreversible structural and magnetic conversions of these compounds by applying hydrostatic pressure of up to 19.8 GPa. The present report is the first one describing the effect of pressure on molecule-based magnets in the GPa region, and this pressure range is over 10 times as large as that of previous studies.

Physical Measurements. X-ray powder diffraction (XRPD) data were collected on a Rigaku RINT 2000 Ultima diffractometer with Cu Kα radiation. Ac and dc magnetic susceptibility measurements under ambient pressure were performed on a Quantum Design MPMS-XL5R SQUID magnetometer in the temperature range of 2−300 K. Crystals of **1**−**3** were well ground and placed in a gelatin capsule, mounted inside straw, and fixed to the end of a sample transport rod. Effective magnetic moments were calculated by the equation $\mu_{eff} = (8\chi_M T)^{1/2}$, where χ_M is the molar magnetic susceptibility corrected for diamagnetism of the constituent atoms. Magnetic measurements under a hydrostatic pressure up to 1.03 GPa were carried out using a piston-cylinder-type of pressure cell (PC) made of Cu−Be alloy, which can be inserted into a Quantum Design SQUID magnetometer. Apiezon-J oil was used as a pressure-transmitting medium. The sample (3−8 mg) was well ground and dispersed into the Apiezon oil with a piece of Pb whose superconducting transition temperature is the probe to estimate the actual pressure at low temperature.[35−38] The mixture was placed in a Teflon bucket and fixed in the clamp cell. A

(22) Milon, J.; Daniel, M. C.; Kaiba, A.; Guionneau, P.; Brandés, S.; Sutter, J. P. *J. Am. Chem. Soc.* **2007**, *129*, 13872.
(23) Nowicka, B.; Rams, M.; Stadnicka, K.; Sieklucka, B. *Inorg. Chem.* **2007**, *46*, 8123.
(24) Yanai, N.; Kaneko, W.; Yoneda, K.; Ohba, M.; Kitagawa, S. *J. Am. Chem. Soc.* **2007**, *129*, 3496.
(25) Ohkoshi, S.; Tsunobuchi, Y.; Takahashi, H.; Hozumi, T.; Shiro, M.; Hashimoto, K. *J. Am. Chem. Soc.* **2007**, *129*, 3084.
(26) Ohkoshi, S.; Arai, K.; Sato, Y.; Hashimoto, K. *Nat. Mater.* **2004**, *3*, 857.
(27) Kurmoo, M.; Kumagai, H.; Chapman, K. W.; Kepert, C. J. *Chem. Commun.* **2005**, 3012.
(28) Maspoch, D.; Ruiz-Molina, D.; Wurst, K.; Domingo, N.; Cavalliano, M.; Biscarini, F.; Tejada, J.; Rovira, C.; Veciana, J. *Nat. Mater.* **2003**, *2*, 190.
(29) Ohba, M.; Ōkawa, H.; Fukita, N.; Hashimoto, Y. *J. Am. Chem. Soc.* **1997**, *119*, 1011.
(30) Kaneko, W.; Ohba, M.; Kitagawa, S. *J. Am. Chem. Soc.* **2007**, *129*, 13706.
(31) Usuki, N.; Ohba, M.; Ōkawa, H. *Bull. Chem. Soc. Jpn.* **2002**, *75*, 1693.
(32) Miyasaka, H.; Ieda, H.; Matsumoto, N.; Re, N.; Crescenzi, R.; Floriani, C. *Inorg. Chem.* **1998**, *37*, 255.
(33) Miyasaka, H.; Matsumoto, N.; Re, N.; Gallo, E.; Ōkawa, H. *Inorg. Chem.* **1997**, *36*, 670.
(34) Larionova, J.; Chavan, S. A.; Yakhmi, J. V.; Frøystein, A. G.; Sletten, J.; Sourisseau, C.; Kahn, O. *Inorg. Chem.* **1997**, *36*, 6374.
(35) Jérome, D.; Schulz, H. J. *Adv. Phys.* **1982**, *31*, 299.
(36) Ishigura, T.; Yamaji, K. *Organic Superconductors*; Springer-Verlag: Heidelberg, Germany, 1990.
(37) Takeda, K.; Mito, M. In *Carbon-Based Magnetism*; Makarova, T., Palacio, F., Eds.; Elsevier: Amsterdam, 2006; p 131.
(38) Mito, M.; Kawae, T.; Takeda, K.; Takagi, S.; Matsushita, Y.; Deguchi, H.; Rawson, J. M.; Palacio, F. *Polyhedron* **2001**, *20*, 1509.
(39) Hosokoshi, Y.; Tamura, M.; Kinoshita, M. *Mol. Cryst. Liq. Cryst.* **1997**, *306*, 423.
(40) Egan, L.; Kamenev, K.; Papanikolaou, D.; Takabayashi, Y.; Margadonna, S. *J. Am. Chem. Soc.* **2006**, *128*, 6034.
(41) Coronado, E.; Giménez-López, M. C.; Levchenko, G.; Romero, F. M.; García-Baonza, V.; Milner, A.; Paz-Pasternak, M. *J. Am. Chem. Soc.* **2005**, *127*, 4580.
(42) Hanawa, H.; Moritomo, Y.; Tateishi, J.; Ohishi, Y.; Kato, K. *J. Phys. Soc. Jpn.* **2004**, *73*, 2759.
(43) Ksenofontov, V.; Levchenko, G.; Reiman, S.; Gütlich, P.; Bleuzen, A.; Escax, V.; Verdaguer, M. *Phys. Rev. B* **2003**, *68*, 024415.
(44) Moritomo, Y.; Hanawa, M.; Ohishi, Y.; Kato, K.; Takata, M.; Kuriki, A.; Nishibori, E.; Sakata, M.; Ohkoshi, S.; Tokoro, H.; Hashimoto, K. *Phys. Rev. B* **2003**, *68*, 144106.
(45) Awaga, K.; Sekine, T.; Okawa, M.; Fujita, W.; Holmes, S. M.; Girolami, G. S. *Chem. Phys. Lett.* **1998**, *293*, 352.
(46) Kaneko, W.; Mito, M; Kitagawa, S.; Ohba, M. *Chem.−Eur. J.* **2008**, DOI: 10.1002/chem.200701364.
(47) Shum, W. W.; Her, J. H.; Stephens, P. W.; Lee, Y.; Miller, J. S. *Adv. Mater.* **2007**, *19*, 2910.
(48) Salah, M. B.; Vilminot, S.; André, G.; Richard-Plouet, M.; Mhiri, T.; Takagi, S.; Kurmoo, M. *J. Am. Chem. Soc.* **2006**, *128*, 7972.
(49) Maeda, T.; Mito, M.; Deguchi, H.; Takagi, S.; Kaneko, W.; Ohba, M.; Ōkawa, H. *Polyhedron* **2005**, *24*, 2497.
(50) Laukhin, V.; Martínes, B.; Fontcuberta, J.; Amabilino, D. B.; Minguet, M.; Veciana, J. *J. Phys. Chem. B* **2004**, *108*, 18441.
(51) Hung, Z. J.; Chen, F.; Ren, Y. T.; Xue, Y. Y.; Chu, C. W.; Miller, J. S. *J. Appl. Phys.* **1993**, *73*, 6563.
(52) Mito, M.; Deguchi, H.; Tajiri, T.; Takagi, S.; Yamashita, M.; Miyasaka, H. *Phys. Rev. B* **2005**, *72*, 144421.
(53) Yamashita, M.; Shimizu, H.; Sakoyama, K.; Manabe, T.; Otsuka, T.; Awaga, K. *Synth. Met.* **1999**, *103*, 2162.
(54) Ohba, M.; Usuki, N.; Fukita, N.; Ōkawa, H. *Angew. Chem., Int. Ed.* **1999**, *38*, 1795.
(55) Kaneko, W.; Ohba, M; Ōkawa, H.; Kitagawa, S. *Inorg. Chem.* **2006**, *45*, 7191.
(56) Ohba, M.; Yamada, M.; Usuki, N.; Ōkawa, H. *Mol. Cryst. Liq. Cryst.* **2002**, *379*, 241.

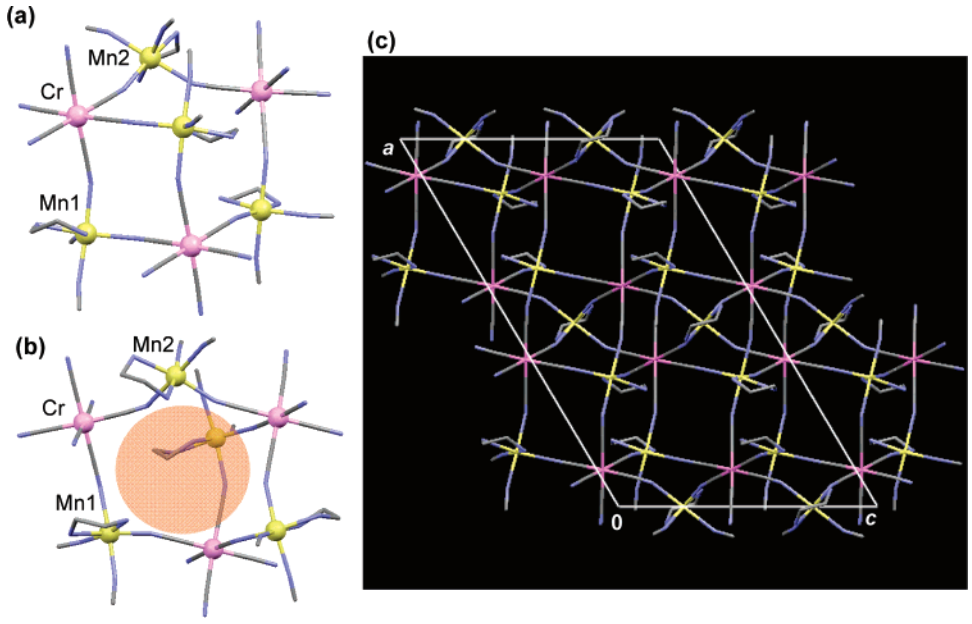

Figure 1. Structure of $[Mn(en)]_3[Cr(CN)_6]_2 \cdot 4H_2O$ (**1**): (a) Cr_3Mn_4 defect cubane unit, (b) a cavity in the cubane unit, and (c) a projection of the framework onto the *ac* plane.

hydrostatic pressure of up to 19.8 GPa was achieved using a diamond anvil cell (DAC),[49,57] which can be inserted into a Quantum Design SQUID magnetometer. The tip diameter of the diamond anvil was 0.5 mm. In the center of the gaskets made of Cu−Be (for $P \leq 5$ GPa) or Re (for $P > 5$ GPa), the sample space with diameter 0.2 mm and height 0.2 mm was holed. The sample of ca. 4 μg and some pieces of ruby were held with a transmitting medium (Daphne oil) in the sample space. The amount of pressure was determined measuring the shift of the R_1 ruby fluorescence at room temperature.[58] The effective pressure in the low-temperature region has been estimated to be at most an increase of ca. 14% of the pressure at room temperature.[57] Because the weight of the sample placed in the PC and DAC could not be measured accurately, the raw data of the measurement were used as magnetization *M*. The XRPD pattern analyses under high pressures were carried out at room temperature using the synchrotron radiation X-ray powder diffractometer with a cylindrical imaging plate at the Photon Factory, Institute of Material Structure Science, High Energy Accelerator Research Organization (KEK), Japan. The wavelength of the incident X-rays was 0.6876(3) Å. Pressure was attained by the use of a DAC with a Be backing plate, on which diamonds with flat tips of 0.6 mm diameter were mounted. There, a CuBe gasket of 200 μm thickness was used. The values of pressure were calibrated with the ruby fluorescence method.[58] In a sample cavity with diameter of 0.2 mm, holed in the center of the gasket, the powdered sample and a few ruby crystals were inserted with a pressure-transmitting medium, fluorine oil (FC70). Through a series of experiments, three kinds of pressure-transmitting media were used as the measurement demand, and each medium worked effectively so as to realize quasi-hydrostatic pressure.

Results and Discussion

Crystal Structures and Magnetic Properties under Ambient Pressure. All compounds have already been reported,[24,54−56] but there has been no detailed comparison of their structures and properties. Their synthesis, crystal structures, and magnetic properties are briefly described below. The crystal structures of **1**−**3** are shown in Figures 1−3. Their crystal parameters are summarized in Table 1, where each density was recalculated with and without lattice water molecules. The solvent-accessible void in each framework is estimated by PLATON[59] in the absence of all lattice water molecules. The dc magnetic susceptibilities of **1**−**3** are shown in Figure 4 in the form of χ_M versus *T*.

$[Mn(en)]_3[Cr(CN)_6]_2 \cdot 4H_2O$ (1). The compound was obtained as stable light-green crystals by the reaction of $MnCl_2 \cdot 4H_2O$, en, and $K_3[Cr(CN)_6]$ in a mole ratio of 3:3:2 under anaerobic conditions. In the crystal structure, the asymmetric unit consists of one $[Cr(CN)_6]^{3-}$ anion, one $[Mn(1)(en)]^{2+}$ cation, one-half of a $[Mn(2)(en)]^{2+}$ cation, and two water molecules. All the cyanide groups of $[Cr(CN)_6]^{3-}$ coordinate to six adjacent Mn atoms (Figure 1). The geometry about the Mn atom is pseudo-octahedral with a chelating en and four cyanide nitrogen atoms. A 3-D network is formed by an alternating array of μ_6-$[Cr(CN)_6]^{3-}$ and $[Mn(en)]^{2+}$, based on a defective cubane having three Cr and four Mn atoms at the seven corners and eight Cr−CN−Mn edges, where the cubane unit lacks one corner and forms an inner cavity. The lattice water molecules are located in the cavity and form hydrogen bonds to each other. The solvent-accessible void is estimated to be 13.9%.

The $\chi_M T$ versus *T* curve showed a gradual decrease from room temperature to a minimum at 156 K because of an antiferromagnetic interaction between the adjacent Mn^{II} and Cr^{III} ions through cyanide bridges and then showed an increase and a long-range ferrimagnetic ordering with $T_C = 69$ K. The $1/\chi_M$ versus *T* plot (156−300 K) obeys the Curie−Weiss law with a negative Weiss constant θ of −38 K. The magnetic hysteresis loop at 2 K showed a typical soft magnetic behavior with coercive field

(57) Mito, M.; Hitaka, M.; Kawae, T.; Takeda, K.; Kitai, T.; Toyoshima, N. *Jpn. J. Appl. Phys.* **2001**, *40*, 6641.
(58) Piermarini, G. J.; Block, S.; Barnett, J. D.; Forman, R. A. *J. Appl. Phys.* **1975**, *46*, 2774.
(59) Spek, A. L. *PLATON*, A Multipurpose Crystallographic Tool; Utrecht University: Utrecht, The Netherlands, 2001.

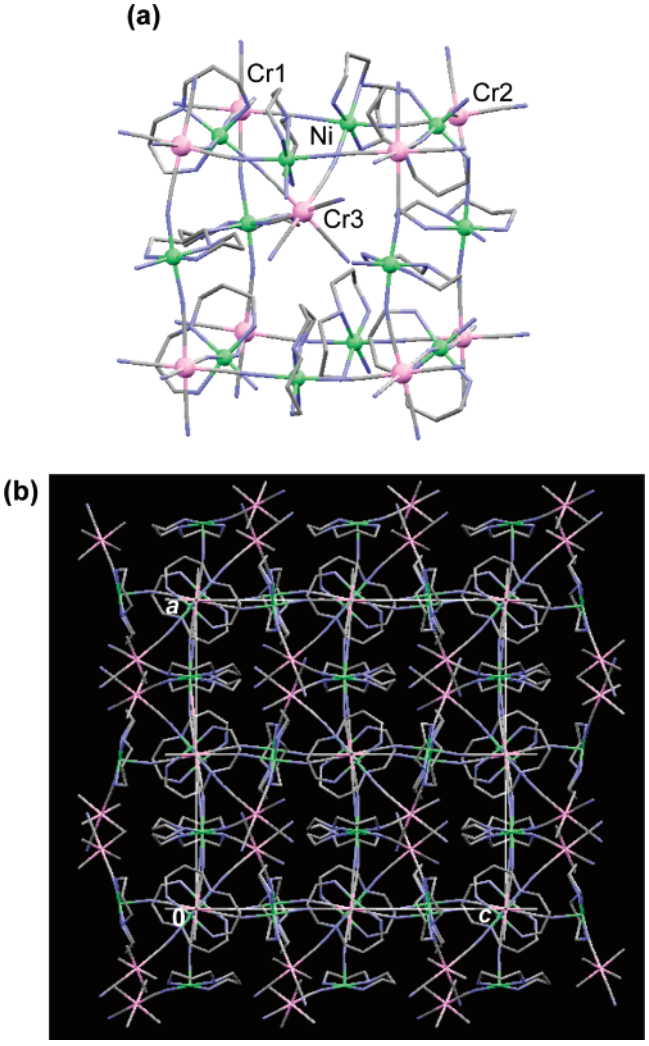

Figure 2. Structure of $[Ni(dipn)]_3[Cr(CN)_6]_2 \cdot 3H_2O$ (**1**): (a) Cr_8Mn_{12} cubane unit with inner $[Cr(3)(CN)_6]^{3-}$, and (b) a projection of the framework onto the *ac* plane.

(H_C) of 30 Oe and saturation magnetization (M_S) value of 8.72 $N\beta$ at 50 kOe.

$[Ni(dipn)]_3[Cr(CN)_6]_2 \cdot 3H_2O$ (2). Compound **2** was obtained as stable purple dodecahedral crystals by the reaction of $NiCl_2 \cdot 6H_2O$, dipn, and $K_3[Cr(CN)_6]$ in a mole ratio of 3:6:2 in an aqueous solution using an H-shaped tube. The nonstoichiometric reaction of the components is necessary to avoid precipitation of the byproduct $Ni_3[Cr(CN)_6]_2 \cdot 15H_2O$. The asymmetric unit of **2** consists of one $[Ni(dipn)]^{2+}$ cation, 1/6 of $[Cr(1)(CN)_6]^{3-}$ and $[Cr(2)(CN)_6]^{3-}$ anions, 1/3 of a $[Cr(3)(CN)_6]^{3-}$ anion, and one water molecule. All the cyanide groups of $[Cr(1)(CN)_6]^{3-}$ and $[Cr(2)(CN)_6]^{3-}$ are involved in the coordination to the axial positions of the adjacent $[Ni(dipn)]^{2+}$ cations. The Ni atom is in a pseudo-octahedral geometry with three amino nitrogen atoms of dipn in meridional positions and three cyanide nitrogen atoms. An isotropic 3-D network is constructed based on a Cr_8Ni_{12} cubane unit formed by the array of μ_6-$[Cr(1)(CN)_6]^{3-}$, $[Ni(dipn)]^{2+}$, and μ_6-$[Cr(2)(CN)_6]^{3-}$ in the cubic crystal system with small void space of 5.0% (Figure 2). One $[Cr(3)(CN)_6]^{3-}$ exists inside the cubane unit and coordinates to an equatorial position of three adjacent $[Ni(dipn)]^{2+}$ cations in the facial μ_3-bridging mode. The $[Cr(3)(CN)_6]^{3-}$ unit seems to act as an internal reinforcement for the Cr_8Ni_{12} cube. Three lattice water molecules are captured in the cubane unit through hydrogen bonding to the terminal cyano nitrogen atoms of $[Cr(3)(CN)_6]^{3-}$ units.

The Ni^{II} and Cr^{III} ions ferromagnetically interact through the cyanide bridges due to a strict orthogonality of the magnetic orbitals. The χ_M value increased with decreasing temperature and showed a ferromagnetic ordering. T_C was determined to be 42 K by ac magnetic susceptibility, weak field magnetization, and a dM/dT plot. The Curie−Weiss plot (80−300 K) gave a positive Weiss constant of +54 K. A typical soft magnetic behavior was observed in the magnetic hysteresis loop at 2 K with a very small H_C of 3 Oe and M_S value of 12.35 $N\beta$ at 50 kOe.

$[Ni(dipn)]_2[Ni(dipn)(H_2O)][Fe(CN)_6]_2 \cdot 11H_2O$ (3). Compound **3** was obtained as efflorescent dark-brown crystals by the reaction of $NiCl_2 \cdot 6H_2O$, dipn, and $K_3[Fe(CN)_6]$ in a 3:3:2 mole ratio in dmf−water solution. One $[Fe(CN)_6]^{3-}$ anion, one $[Ni(1)(dipn)]^{2+}$ cation, one-half of a $[Ni(2)(dipn)(H_2O)]^{2+}$ cation, and lattice water molecules constitute the asymmetric unit. Three equatorial cyanide groups of $[Fe(CN)_6]^{3-}$ coordinate to three adjacent $[Ni(1)(dipn)]^{2+}$ cations, and one axial cyanide group coordinates to the axial position of the adjacent $[Ni(2)(dipn)(H_2O)]^{2+}$ cation. Both Ni ions are in a pseudo-octahedral geometry with dipn in meridional mode and three cyanide nitrogen atoms for Ni(1), and with dipn in meridional mode, two cyanide nitrogen atoms and one water molecule for Ni(2). In the lattice, the arrays of μ_4-$[Fe(CN)_6]^{3-}$ and $[Ni(1)(dipn)]^{2+}$ form a 2-D sheet on the *bc* plane, and the Fe−CN(2)−Ni(2) linkages connect the 2-D sheets along the *a* axis to construct a 3-D porous pillared-layer framework with a solvent-accessible void of 28.2% (Figure 3). The lattice water molecules reside in a disorderly manner in the pore, and their positions were not determined completely. The crystallinity was readily lost by evacuation.

The $\chi_M T$ versus T plot showed a slight decrease upon cooling to 180 K because of an orbital contribution from the ground state of low-spin Fe^{III} ($^2T_2$). Then the $\chi_M T$ value gradually increased down to 20 K and rapidly increased below 10 K, in which a ferromagnetic interaction operated between Ni^{II} and low-spin Fe^{III} ions through cyanide bridges due to the strict orthogonality of the magnetic orbitals. A long-range ferromagnetic ordering was observed below T_C of 8.5 K. The Curie−Weiss plot (20−300 K) gave a small positive Weiss constant of +5.3 K, including a small negative contribution from spin−orbit coupling. A magnetic hysteresis was observed at 2 K with H_C of 350 Oe and M_S of 8.03 $N\beta$ at 50 kOe.

It is obvious that the structural strength of these frameworks is in the order **3** < **1** < **2** from an architectural viewpoint. To evaluate the strength numerically, the density and solvent-accessible void of each crystal excluding the lattice water molecules were estimated (Table 1). The values well support the order of the structural strength. In fact, the 3-D pillared-layer structure of **3** is very fragile and easily changed to an amorphous phase by dehydration, whereas frameworks **1** and **2** are stable to dehydration. The structural strength is closely related to the pressure response discussed below.

Structural Stability under Pressure. To confirm the structural changes and the stability under pressure, X-ray powder diffraction (XRPD) was performed in the pressure range of 0−4.7 GPa using DAC (Figure 5).

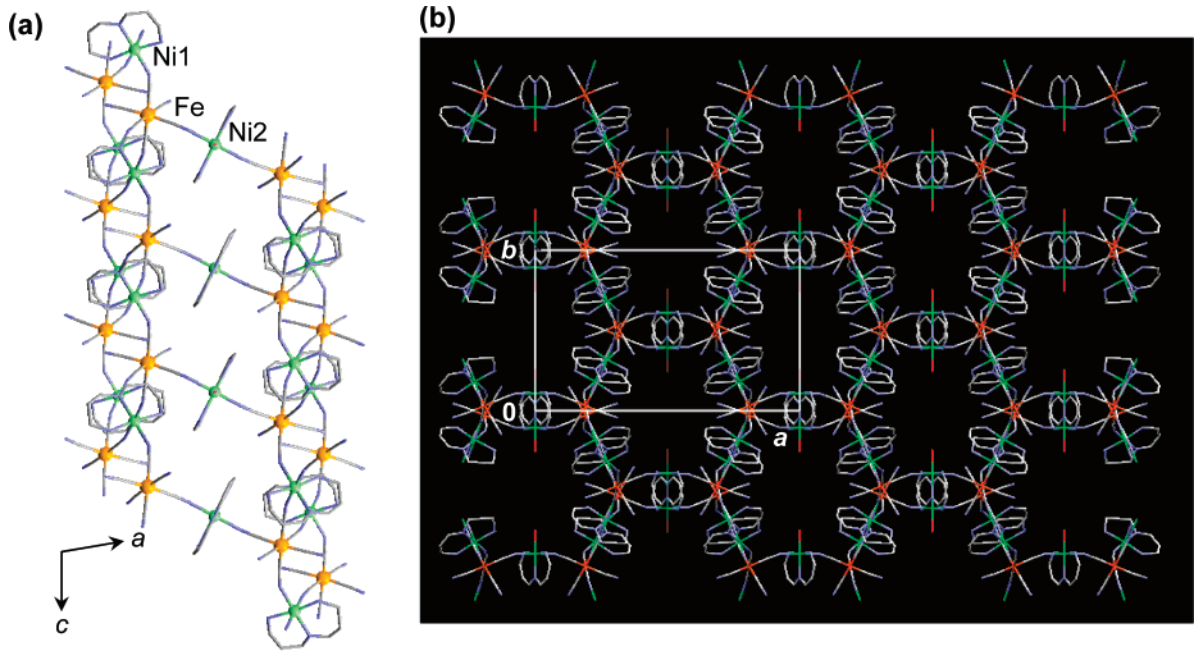

Figure 3. Structure of $[Ni(dipn)]_2[Ni(dipn)(H_2O)][Fe(CN)_6]_2 \cdot 11H_2O$ (**3**): (a) a pillared-layer structure, and (b) a projection of the framework onto the *ab* plane.

Table 1. Crystal Parameters of 3-D Cyanide-Bridged Magnets **1**−**3**, **a** and **b**

compound	MnCr (**1**)	NiCr (**2**)	NiFe (**3**)	MnCr (**a**)	MnMn (**b**)
formula weight	833.37	1040.01	1209.86	2227.20	2233.09
No. of lattice water	4	3	11	10	10
crystal system	monoclinic	cubic	monoclinic	trigonal	trigonal
space group	*C*2/c	*Pa*$\bar{3}$	*C*2/*c*	*R*$\bar{3}$	*R*$\bar{3}$
a/Å	24.505(7)	20.9742(7)	24.044(8)	38.759(9)	38.46(1)
b/Å	11.323(4)	20.9742(7)	14.343(4)	38.759(9)	38.46(1)
c/Å	14.810(4)	20.9742(7)	16.688(5)	20.559(5)	20.287(6)
α/°	90	90	90	90	90
β/°	120.96(2)	90	100.552(4)	90	90
γ/°	90	90	90	120	120
V/Å^3	3533(1)	9226.90(1)	5657(3)	26747.2(8)	25982(12)
Z	4	8	4	9	9
D_{calcd}/g•cm^{-3}	1.566	1.601	1.421	1.244	1.284
D_{calcd}/g•cm^{-3} (without lattice water)	1.431	1.420	1.188	1.144	1.181
solvent-accessible void/%	13.9	5.0	28.2	13.7	12.9
ref	54	55	24	46	46

In the case of **1**, four peaks were observed in the 2θ range of 6−10° and assigned to (0 2 0), (0 2 1), (3 1 1), and (2 0 2) starting from the low angle. These diffraction patterns were analyzed by a Rietveld method with accuracy as *R*wp = 1.6−2.6% and *S* = 1.4−2.0.[60,61] The contribution of diamond anvils and fluorine oil (FC70) was considered as background data. The peaks gradually broadened with increasing pressure. The lattice contracted in an isotropic manner for $P \leq 1.7$ GPa, and the lattice volume linearly decreased. At higher pressure, the *bc* frame and total volume hardly changed, but the stacking along the *a* axis tended to tilt with the expansion of the *a* axis anisotropically. The change of lattice size leveled off with a volume decrease of ca. 9% at 3.2 GPa (Figure 6a). Above 4.2 GPa, an amorphous-like pattern finally appeared. However, there the network of magnetic correlation is surprisingly maintained (see next section). After releasing pressure at 4.5 GPa, the initial crystalline phase was recovered, which indicates that the framework extended by Cr−CN−Mn linkages had sufficient elasticity.

On the other hand, compound **2** showed a quite different response to pressure in the 2θ range of 3−10° (Figure 5b). Main peaks were assigned to (2 0 0), (2 2 2), (4 0 0), (4 2 0) and (2 4 0) starting from a low angle. The Rietveld analysis well simulated these diffraction patterns with *R*wp = 3.6−4.3% and *S* = 2.5−3.2. The cell volume was linearly and isotropically decreased in the range of 0−3.1 GPa and finally compressed by ca. 15% at 4.7 GPa with broadening of the peaks and without amorphization, which demonstrated the structural strength of **2** (Figure 6b). The shrinkage ratio of **2** is about twice as large as that of **1**. In the case of **3**, the XRPD pattern was easily changed to an amorphous-like pattern by dehydration under ambient pressure.

Pressure Dependence of Magnetic Susceptibility. The static magnetic susceptibilities of **1**−**3** under various hydrostatic pressures (up to 19.8 GPa) are shown in Figures 7−10, 12, and

(60) Kim, Y.-I.; Izumi, F. *J. Ceram. Soc. Jpn.* **1994**, *102*, 40.
(61) Izumi, F. In *The Rietveld Method*; Yong, R. A., Ed.; Oxford University Press: Oxford, 1993; Chapter 13.

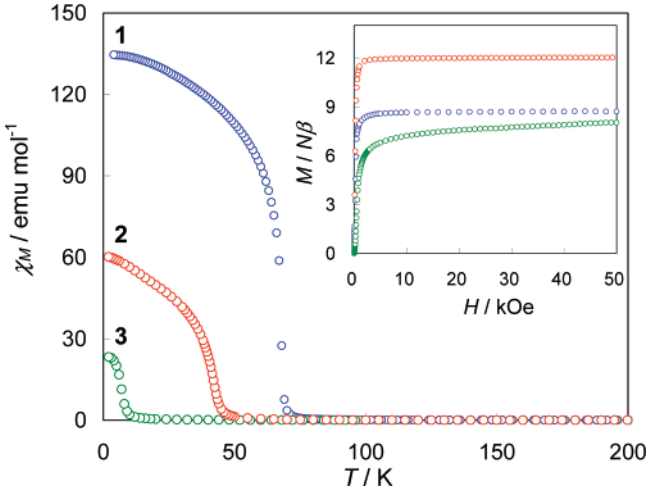

Figure 4. Temperature dependences of molar magnetic susceptibility χ_M for $Mn^{II}Cr^{III}$ ferrimagnet (**1**: blue), $Ni^{II}Cr^{III}$ ferromagnet (**2**: red), and Ni^{II}-Fe^{III} ferromagnet (**3**: green). The inset shows the field dependences of magnetization M for **1** (blue), **2** (red), and **3** (green).

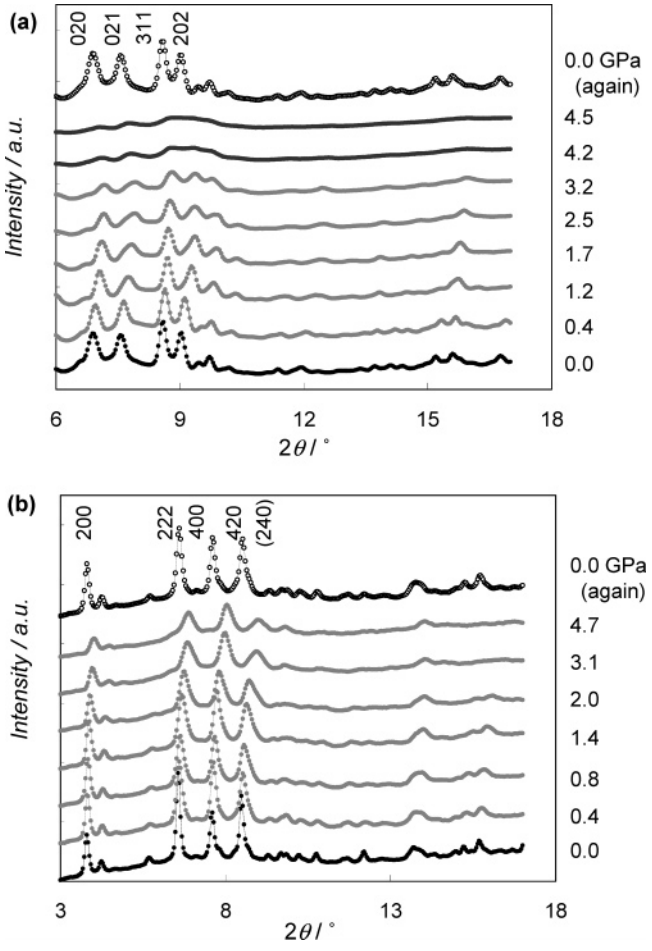

Figure 5. XRPD patterns of **1** (a) and **2** (b) at various pressures.

13 in the form of M versus T plots, where M is the magnetization. The hydrostatic pressure up to 1.03 GPa was applied using a PC employing Apiezon grease J as a pressure-transmitting medium, and the effective pressure at low temperature was calibrated using the superconducting transition of Pb. The magnetization of Pb vanished on applying a dc magnetic field of 1 kOe (critical field at $T = 0$ is ca. 0.8 kOe). A higher hydrostatic pressure up to 19.8 GPa was applied by a DAC with

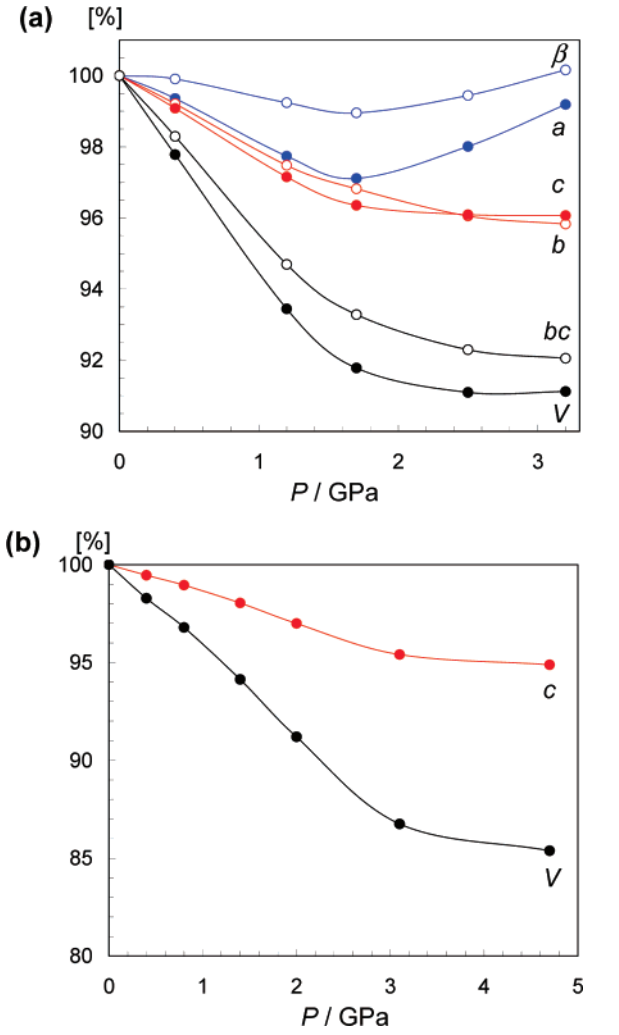

Figure 6. Pressure dependences of lattice parameters of **1** (a) and **2** (b) based on the Rietveld analysis: a axis (●, blue), b axis (○, red), c axis (●, red), β (○, blue), V (●, black) and bc frame (○, black).

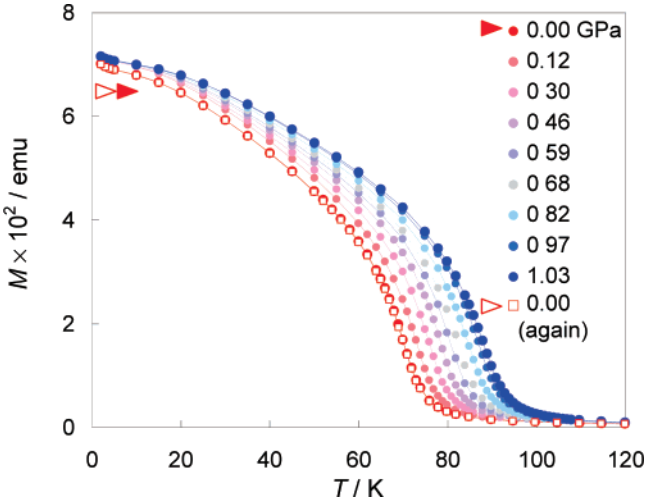

Figure 7. Temperature dependences of the magnetization (M) of **1** at various hydrostatic pressures using a PC.

a small sample space (diameter of 0.2 mm) in the Cu−Be or Re gaskets. The amount of pressure was monitored by the shift of the R_1 ruby fluorescence at room temperature. All the magnetization values were measured under a dc magnetic field of 5 kOe, which is sufficient to saturate the magnetic moment

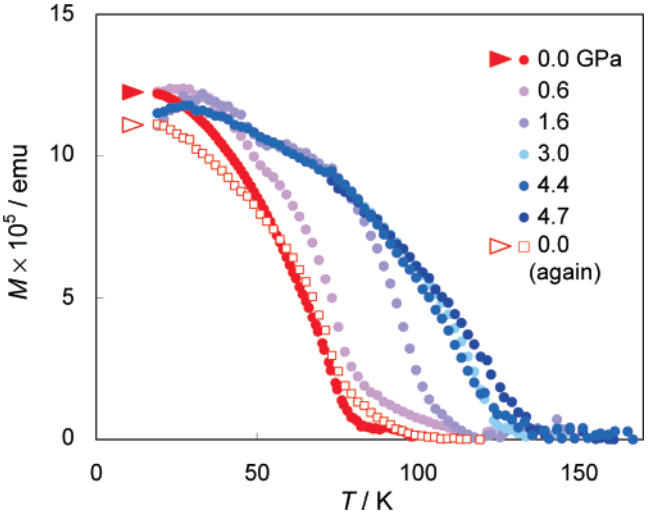

Figure 8. Temperature dependences of the magnetization (M) of **1** in the pressure range $0 \leq P \leq 4.7$ GPa using a DAC.

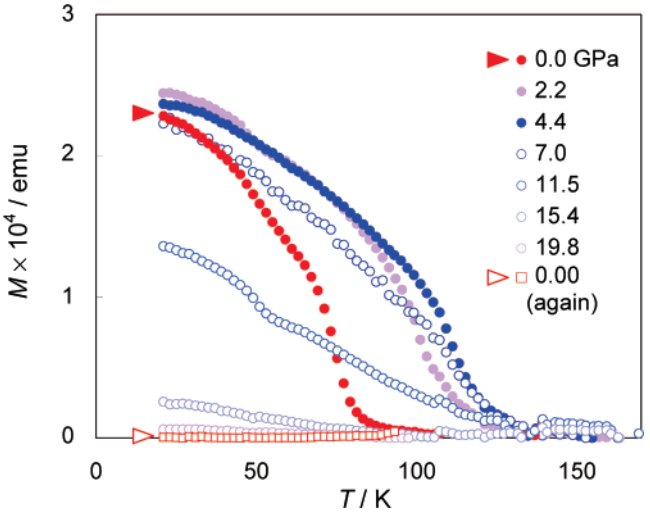

Figure 9. Temperature dependences of the magnetization (M) of **1** in the pressure range $0 \leq P \leq 19.8$ GPa using a DAC.

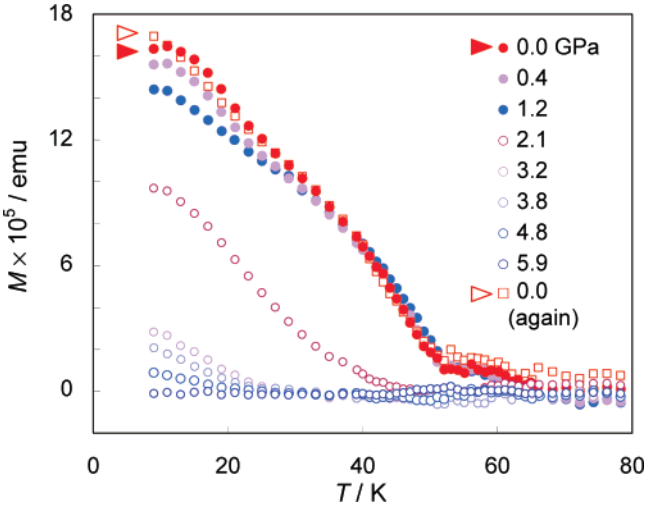

Figure 10. Temperature dependence of the magnetization (M) of **2** in the pressure range $0 \leq P \leq 5.9$ GPa using a DAC.

in the ordered state of each compound. Then the measurement sensitivity is not enough to discuss the paramagnetic behavior quantitatively but can have us mention the temperature dependence of the ferromagnetic moment. In all cases, the reversibility in the magnetic behavior was validated by releasing the pressure after successive measurements up to the maximum pressure.

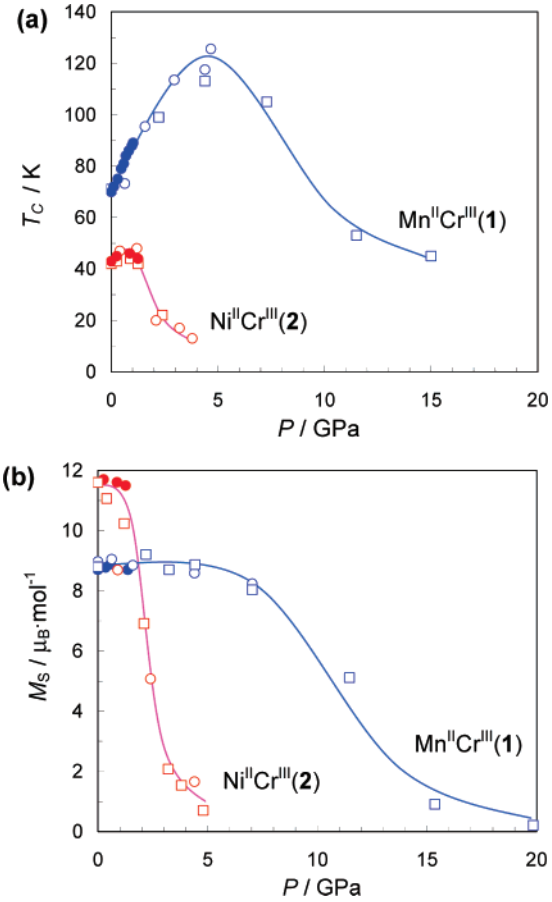

Figure 11. Pressure dependences of T_C for **1** and **2** (a), and the maximum magnetization value (M_S) for **1** and **2** (b). Compound **1**: ● (blue) (PC), ○ (blue) (DAC, first run), □ (blue) (DAC, second run); **2**: ● (red) (PC), ○ (red) (DAC, first run), □ (red) (DAC, second run). Solid curves are guides.

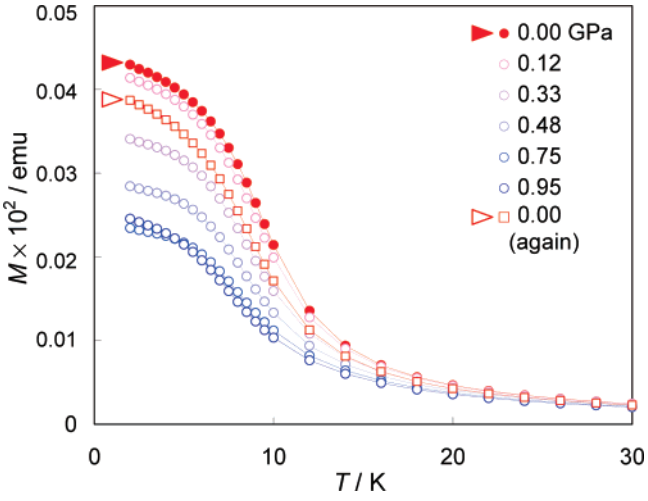

Figure 12. Temperature dependences of the magnetization (M) of **3** in the pressure range $0 \leq P \leq 0.95$ GPa using a PC.

$[Mn(en)]_3[Cr(CN)_6]\cdot 4H_2O$ (1). Figure 7 shows the pressure dependence of magnetization M under an applied field of 5 kOe in the pressure region of 0−1.03 GPa obtained with the PC. The M versus T curve of **1** under ambient pressure corresponds to the χ_M versus T curve shown in Figure 4. The curve gradually

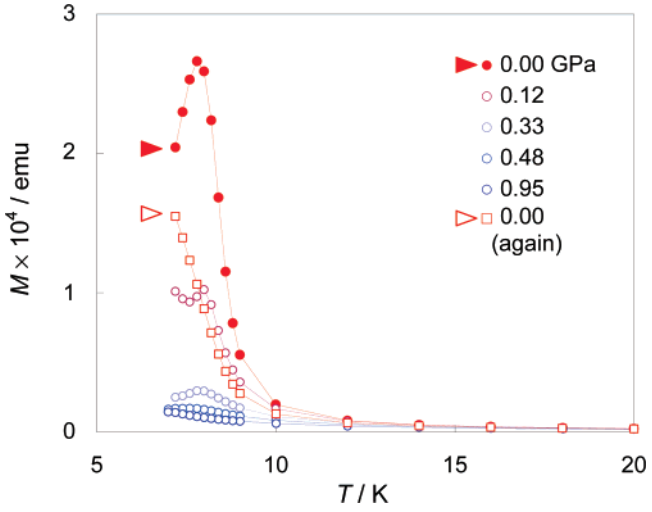

Figure 13. Temperature dependences of the in-phase magnetization (M') of **3** in an ac field of 3 Oe at a frequency of 10 Hz, under various pressures.

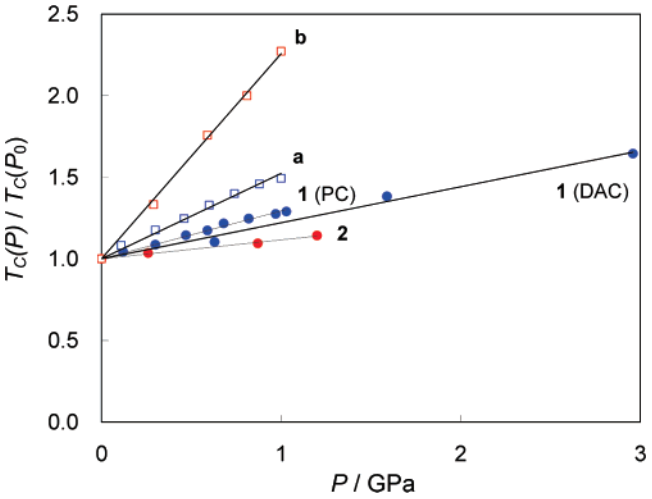

Figure 14. Pressure dependence of $T_C(P)/T_C(P_0)$ of **1** (●, blue), **2** (●, red), **a** (□, blue), and **b** (□, red). As for each compound, only the data showing the linear pressure dependence are picked out.

shifted toward higher temperatures with increasing pressure. The T_C was determined from a dM/dT plot and the ac magnetic response in an ac field of 3 Oe at a frequency of 10 Hz. The value of T_C linearly increased from 69 K at 0 GPa to 89 K at 1.03 GPa. The initial magnetic behavior was completely recovered after releasing the pressure. The pressure dependence of T_C clearly demonstrates the linear relationship of T_C with the applied pressure, with $dT_C/dP = +19.4$ K·GPa^{-1}. To evaluate the pressure effects, the rate of T_C change (the initial slope a) was estimated by eq 1:[37]

$$T_C(P) = (1 + aP) \times T_C(P_0) \quad (1)$$

where $T_C(P_0)$ is T_C at ambient pressure.

In the case of **1**, the initial slope a was estimated to be 0.28 GPa^{-1}, where $T_C(P_0) = 69$ K and $T_C(1.03) = 89$ K (Figure 14). The increase in T_C resulting from the external pressure reflects the increase of overlap integrals between dπ(Cr^{III}) and π^*(CN^-) and between dπ(Mn^{II}) and π^*(CN^-) orbitals, accompanied by a shrinkage of the Cr−CN−Mn linkages.[45,49]

Under higher pressure, the T_C reached 126 K at 4.7 GPa (Figure 8), in which the value of T_C was determined by the dM/dT plot. For $P \leq 3.0$ GPa, T_C linearly increased to 114 K at 3.0 GPa with $dT_C/dP = +15.0$ K·GPa^{-1} and an a value of 0.22 GPa^{-1}. The enhancement of T_C was saturated in the range $3.0 \leq P \leq 4.7$ GPa (Figure 11a). The magnetic behavior after releasing the pressure at 4.7 GPa was essentially coincident with that of the initial state. The saturation magnetization shows no significant changes in the range $0 \leq P \leq 4.7$ GPa (Figure 11b). The magnetic reversibility is consistent with the structural reversibility. These results show that compound **1** maintains the ferrimagnetic phase without decreasing the saturation magnetization value (no fragmentation of the magnetic domain) even in the amorphous phase. Under higher pressure, $P \geq 4.7$ GPa, T_C and saturation magnetization decreased with increasing pressure (Figures 9 and 11). Finally, the ferrimagnetic phase vanished and a paramagnetic-like phase appeared at 19.8 GPa. These changes arise from the reduction of domain size, and similar behavior has also been seen in the process of synthesizing nano-size particles of the Fe/Cr−CN−Co Prussian-blue-type analogue.[62] After releasing pressure at 19.8 GPa, only a paramagnetic-like phase was observed, and the initial magnetic behavior was not recovered. The irreversible magnetic change and the decrease of magnetization imply further amorphization and a collapse of the framework.

$[Ni(dipn)]_3[Cr(CN)_6]_2\cdot 3H_2O$ (2). The pressure dependence of magnetization M under an applied field of 5 kOe in the pressure region of 0−5.9 GPa measured with the DAC is given in Figure 10. The value of T_C slightly increased from 42 K at 0 GPa to 48 K at 1.2 GPa with $dT_C/dP = +5.0$ K·GPa^{-1} and an a value of 0.12 GPa^{-1}, and then decreased. Above 1.2 GPa, the M versus T curve shifted to lower temperature and the saturation magnetization value immediately decreased with increasing pressure, and finally, paramagnetic-like behavior appeared at 4.8 GPa, although **2** keeps its crystallinity in the pressure range (Figure 11). The magnetic behavior is the same as **1** under $P \geq 15$ GPa. In the case of the ferromagnet **2**, the external pressure gave a negative contribution to the magnetic ordering, in contrast to the ferrimagnet **1**. Shrinkage of the framework would induce a bend in the Cr−CN−Ni linkages, which increases orbital overlapping and breaks the strict orthogonality between magnetic orbitals of Cr^{III} and Ni^{II}. This structural change is interestingly quite subtle and has a significant influence on magnetic properties. At the present stage, a direct proof cannot be obtained through XRPD under pressure, due to the difficulty of determining each atom position. After releasing the pressure at 5.9 GPa, the initial behavior was completely regenerated, which represented that compound **2** was reversibly switched between the ferromagnetic and the paramagnetic-like phases by the external pressure.

$[Ni(dipn)]_2[Ni(dipn)(H_2O)][Fe(CN)_6]_2\cdot 11H_2O$ (3). M versus T plots of ferromagnet **3** in the pressure range of 0−0.95 GPa are given in Figure 12. No increase of T_C was observed upon applying pressure. The M versus T curve shifted toward lower temperatures, and the magnetization value decreased with increasing pressure. No cusp of in-phase and out-of-phase magnetization was observed in the range for $P \geq 0.48$ GPa (Figure 13). After releasing the pressure at 0.95 GPa, the M versus T curve did not trace the initial curve, and the M' versus T plot did not reproduce the cusp. These facts imply a collapse

(62) Yamada, M.; Arai, M.; Kurihara, M.; Sakamoto, M.; Miyake, M. *J. Am. Chem. Soc.* **2004**, *126*, 9482.

Scheme 1

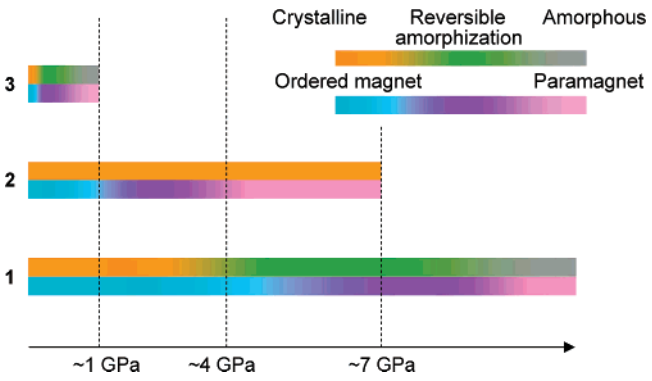

of the framework or magnetic domain fragmentation. Similar to **2**, shrinkage of the Fe−CN−Ni linkages contributed negatively to the ferromagnetic interaction. Furthermore, the framework was irreversibly changed by low pressure because of the anisotropic and porous framework. The porous framework of **3** sensitively responds to the external pressure, but it is too fragile to maintain reversibility.

The systematic magnetic results of **1**−**3** providing the same M−CN−M′ linkages highlighted a significant difference of the pressure responses depending on the magnetic structure (ferrimagnetic and ferromagnetic) and on the shapes of frameworks (structural strength). The pressure dependences of magnetic and structural phases are depicted in Scheme 1. The borders of the magnetic and structural phases were not defined clearly in Scheme 1 because these changes are not the first-order transition and different phases are coexistent widely in both magnetic (ordered magnet and paramagnet) and structural (crystalline and amorphous) phases.

The effect of pressure on other cyanide-bridged CPMs, $[Mn(4dmap)]_3[M(CN)_6]_2\cdot 10H_2O$ (M = Cr (**a**) and Mn (**b**); 4-dmap = 4-dimethylaminopyridine), was recently reported by us.[46] These compounds also give significant information on the pressure response of the cyanide-bridged CPMs. Compounds **a** and **b** form a cyanide-bridged twofold interpenetrated 3-D network based on three-way connected $6,10^2$ nets. These compounds demonstrate good reversible pressure response in the range of 0−1.00 GPa. Here we discuss the pressure dependence of T_C using the a value in eq 1, $T_C = (1 + aP) \times T_C(P_0)$. The a values of **a** and **b** were estimated to be 0.49 GPa^{-1} ($T_C(P_0)$ = 17.0 K and $T_C(1.00)$ = 25.4 K) and 1.29 GPa^{-1} ($T_C(P_0)$ = 6.4 K and $T_C(1.04)$ = 15.0 K), respectively. This a value can be treated as showing a substantial compressibility from the magnetic aspects. Comparing the $Mn^{II}Cr^{III}$ ferrimagnets **1** and **a**, the a value of **a** is higher than that of **1** because **a** and **b** have a more flexible framework with low density (see Table 1 and Figure 14). In addition, the a value of **b** is much higher than those of the other compounds, which suggests that the magnetic interaction pathway including magnetically anisotropic Mn^{III} ions in the C_{2v} symmetry structure was made more effective by structural compression. Judging from the density, the frameworks of **a** and **b** seem to be fragile as well as the porous framework of **3**. However, **a** and **b** demonstrate good structural and magnetic reversibility, which suggests that the interpenetrated structure decreasing the void space in the framework prevents collapse (amorphization) of the framework and plays a significant role for the reversible response to mechanical stress. Recently, Miller et al. reported a similar pressure-dependent reversible enhancement of T_C for the 3-D interpenetrated cubic ferrimagnet, $[Ru_2(O_2CCH_3)_4]_3[Cr(CN)_6]$ (**c**).[47] In this case, the T_C value increased from 33 to 59 K at 1.28 GPa (a = 0.62 GPa^{-1}). This compound also shows high response and good reversibility to the external pressure, which supports the utility of flexible cyanide-bridged linkages and interpenetrating frameworks.

In addition, pressure effects on other CPMs, $Mn_3[Mn(CN)_6]_2\cdot 12H_2O\cdot 1.7CH_3OH$ (**d**),[45] $Co_5(OH)_6(SO_4)_2(H_2O)_4$ (**e**),[48] and (*R*)-3MLNN-Mn(hfac)$_2$ (**f**; Hhfac = hexafluoroacetylacetone),[50] have already been reported. The results are summarized in Table 2. Prussian blue analogue **d** forms a face-centered-cubic structure with structural defects, where the average structure is close to that of **1**. In the case of **d**, the $T_C(P_0)$ value of 29 K increased to 40 K at 1.00 GPa, which gave an a value of 0.38 GPa^{-1}. The a value is higher than that of **1**, which would be associated with the structural isotropy, hardness, and the existence of the magnetically anisotropic Mn^{III} ion. Compound **e** forms a 3-D pillared-layer structure based on μ_3-OH-bridged Co^{II} layers and $[Co^{II}(H_2O)_4(SO_4)_2]^{2-}$ pillars and gives an a value of 0.097 GPa^{-1} ($T_C(P_0)$ = 12.6 K and $T_C(0.98)$ = 13.8 K). The low a value of **e** reflects its structural hardness and well-separated 2-D magnetic structure. Compound **f** has a 1-D chain structure based on the alternating array of [Mn(hfac)$_2$] and chiral α-nitronyl nitroxide radical ((*R*)-3MLNN) and shows a ferrimagnetic ordering at 4.7 K.[50] The a value of **f** was estimated to be 0.22 GPa^{-1} ($T_C(P_0)$ = 4.7 K, $T_C(0.98)$ = 5.7 K in 120 Oe), which is comparable in magnitude to the 3-D ferrimagnet **1**. A charge-transfer-type ferromagnet, $[Fe(C_5Me_5)_2][TCNE]$ (**g**),[51] having a 1-D chain structure based on the alternating array of donor and acceptor units shows good compressibility with an a value of 0.45 GPa^{-1} ($T_C(P_0)$ = 4.8 K and $T_C(1.06)$ = 7.1 K). The 1-D donor−acceptor column structure is essentially the same

Table 2. The Values of T_C and the Initial Slope a of Compounds **1**, **2**, and **a**−**h**

compound	$T_C(P_0)$/K	$T_C(P)$/K[a] (P/GPa)	dT_C/dP/K·GPa^{-1}	a/GPa^{-1}	ref
$[Mn(en)]_3[Cr(CN)_6]_2\cdot 4H_2O$ (**1**)	69	89 (1.03)	19.4	0.28	this work
	69	114 (2.96)	15.0	0.22	this work
$[Ni(dipn)]_3[Cr(CN)_6]_2\cdot 3H_2O$ (**2**)	42	48 (1.20)	5.0	0.12	this work
$[Mn(4dmap)_4]_2[Cr(CN)_6]_3\cdot 10H_2O$ (**a**)	17.0	25.4 (1.00)	8.4	0.49	46
$[Mn(4dmap)_4]_2[Mn(CN)_6]_3\cdot 10H_2O$ (**b**)	6.4	15.0 (1.04)	8.3	1.29	46
$[Ru_2(O_2CCH_3)_4]_3[Cr(CN)_6]$ (**c**)	33	59 (1.28)	20.3	0.62	47
$Mn_3[Mn(CN)_6]_2\cdot 12H_2O\cdot 1.7CH_3OH$ (**d**)	29	40 (1.00)	11.0	0.38	45
$Co_5(OH)_6(SO_4)_2(H_2O)_4$ (**e**)	12.6	13.8 (0.98)	1.2	0.097	48
(*R*)-3MLNN-Mn(hfac)$_2$ (**f**)	4.7	5.7 (0.98)	1.0	0.22	50
$[Fe(C_5Me_5)_2][TCNE]$ (**g**)	4.8	7.1 (1.06)	2.2	0.45	51
p-NCC_6F_4CNSSN (**h**)	36	72 (1.64)	21.9	0.61	37, 38

[a] The values of $T_C(P)$ were picked in the end of the linear pressure-dependent region.

as that of organic magnets, which is convenient for compression. However, in the case of organic magnets, the ordered magnetic phase often vanishes upon stressing because of enhancement of the intermolecular antiferromagnetic interaction.[37] A pure organic weak ferromagnet, the β-phase of 1,2,3,5-dithiadiazol-3-yl-4-(4-cyano-2,3,5,6-tetrafluorophenyl) radical (p-NCC_6F_4-CNSSN (**h**)), providing the highest T_C value among genuine organic magnets, gives a high a value of 0.61 GPa^{-1} ($T_C(P_0) =$ 36 K, $T_C(1.64) =$ 72 K).[37,38] The significant increase of T_C results from the enhancement of the antiferromagnetic interaction due to the increase in the SOMO−SOMO overlap. These results clearly demonstrate the significant correlation between packing structure, electronic structure, and pressure response. In particular, for the low-dimensional magnetic system, the spatial margin between frameworks plays an important role for high compression. Further systematic studies will give significant insights for attaining more sensitive and more efficient pressure response.

Conclusion

Pressure effects on structure and magnetic properties of three types of 3-D cyanide-bridged coordination polymer magnets were systematically examined under hydrostatic pressures up to 19.8 GPa. This is the first report of the pressure effect on molecule-based magnets in the GPa region. The T_C of a ferrimagnet $[Mn(en)]_3[Cr(CN)_6]_2 \cdot 4H_2O$ (**1**) increased from 69 K to a maximum value of 126 K at 4.7 GPa. The ferrimagnetic behavior was reversibly changed in the range $0 \leq P \leq 5$ GPa, although the framework was amorphized above 4.2 GPa. In contrast, the T_C decreased at higher pressure, and **1** was irreversibly changed to paramagnetic-like behavior at 19.8 GPa. A ferromagnet $[Ni(dipn)]_3[Cr(CN)_6]_2 \cdot 3H_2O$ (**2**) showed a paramagnetic-like behavior for $P \geq 4.8$ GPa without significant increase of T_C and even maintained crystallinity, where these changes were reversible in the range $0 \leq P \leq 5$ GPa. The pressure dependences of the XRPD patterns in the range $0 \leq P \leq 5$ GPa clearly demonstrate sufficient and unique elasticity of **1** and **2**. A porous ferromagnet $[Ni(dipn)]_2[Ni(dipn)(H_2O)][Fe(CN)_6]_2 \cdot 11H_2O$ (**3**) was easily amorphized and irreversibly lost the ferromagnetic phase under low pressure ($P \leq 1$ GPa). These results were carefully compared with previously reported results based on the compressibility. This review highlights that (1) the mechanical stress provides a positive effect on ferrimagnets and a negative effect on ferromagnets due to shrinkage of the bridging structure and concomitant increase of antiferromagnetic contribution, and (2) the spatial margin and strength of frameworks are significant for high responsivity and reversibility.

Acknowledgment. This work was supported by ERATO JST Project "Kitagawa Integrated Pore Project", Riken Project "Quantum Order Research Program", a Grant-In-Aid for Scientific Research Program (No. 18750046), and CREST JST Program from the Ministry of Education, Culture, Sports, Science and Technology of Japan. W.K. is grateful to JSPS Research Fellowships for Young Scientists.

Supporting Information Available: X-ray crystallographic data of **1**−**3** as CIF. This material is available free of charge via the Internet at http://pubs.acs.org.

JA7110509